Hypoxic conditioning induced by $CoCl_2$ enhanced the therapeutic effects of mesenchymal stem cell-derived exosomes on oxazolone-induced atopic dermatitis-like skin lesions

Jin-Woo Kim
Seoul National University
Hyunji Lee
INEXOPLAT
Jung Min Lee
jm.lee@handong.edu

INEXOPLAT
Jin-Chul Kim
Korea Institute of Science and Technology (KIST)

Article

Keywords: hypoxic condition, mesenchymal stem cells, exosome, anti-inflammation, anti-atopic dermatitis

Posted Date: March 17th, 2024

DOI: https://doi.org/10.21203/rs.3.rs-3968522/v1

Additional Declarations: No competing interests reported.

Abstract

Atopic dermatitis (AD) is a chronic skin disease characterized by inflammation and disruption of the skin barrier. It is normally treated using moisturizers and steroids; however, these are palliatives and do not serve as a therapy. Mesenchymal stem cells (MSCs) are tissue stem cells with immunomodulatory activities, and exosomes are extracellular vesicles that reflect the physiologies of producer cells. Therefore, the use of MSCs and exosomes with their immunomodulatory activities is emerging as a new method to treat AD. Here, we used cobalt chloride ($CoCl_2$) to induce hypoxic conditioning, and tested the therapeutic efficacy of exosomes derived from $CoCl_2$-treated MSCs in treating AD. *In vitro*, the exosomes derived from $CoCl_2$-treated MSCs increased the proliferation of HaCaT cells and decreased inflammatory cytokine levels. In the oxazolone-induced chronic AD mouse model, the exosomes derived from $CoCl_2$-treated MSCs reduced ear thickness, restored the skin barrier, and reduced immune cell infiltration and inflammatory markers. These data indicated that hypoxic conditioning induced by the $CoCl_2$ treatment enhanced the therapeutic efficacy of exosomes derived from MSCs, suggesting that these exosomes can be used to alleviate the symptoms of AD.

Introduction

Atopic dermatitis (AD) is an inflammatory skin disease occurring worldwide and affecting up to 20% of children and 3% of the adult population [1–3]. Persistent exposure of the skin to allergens stimulates skin-resident mast cells and macrophages, the main cell types involved in antigen-specific inflammation [4]. Following stimulation, mast cells activate leukocytes. The activated leukocytes infiltrate into the skin [5], secreting the interleukin-4 (IL-4) and IL-17 cytokines, which lead to the disruption of the skin barrier and upregulation of antimicrobial proteins. Once the skin barrier is disrupted, keratinocytes secrete chemokines and cytokines, which activate T helper 2 (Th2) cell-mediated immune responses [6]. The IL-4 and IL-13 cytokines produced by Th2 cells stimulate immunoglobulin E (IgE) production by B cells [7]. Sensitization to allergens due to elevated IgE levels causes hypersensitivity, which leads to itching and further weakening of the skin barrier [8]. In addition, rapid recall responses are triggered by the generated T-resident memory cells, exacerbating the vicious cycle of inflammation [9]. Therefore, reestablishing the skin barrier and reducing inflammation are crucial for the treatment of AD. Normally, the condition is treated using moisturizers and steroids. Corticosteroid drugs, such as dexamethasone, have also been used to reduce AD pathophysiology for 40 years [10]. However, these treatments are only palliatives and not therapies. In addition, it should be noted that long-term steroid treatments disrupt the patient's hormonal balance and cause severe side effects [11].

MSCs have immunomodulatory and regenerative functions [12, 13]. Numerous studies have shown that MSCs can be recruited to the wounded sites, where they exert their therapeutic effects [14] by reducing inflammation [15] and replacing damaged tissues. Because of their therapeutic activities, MSCs are being studied as new agents to treat inflammation-induced diseases such as AD [16]. However, despite many advantages, the use of MSCs as a therapy implies a number of risks, such as graft-versus-host disease,

differentiation into unwanted cell types, and transformation into tumors after transplantation [17], which impede the clinical application of these cells. Exosomes are nanosized extracellular vesicles that are secreted by cells [18]. They are membrane-bound and contain cellular components, such as DNA, RNA, miRNA, mRNA, and cytokines [19]. Because the composition and concentration of these cellular components reflect the physiologies of producer cells, MSC-derived exosomes exhibit the same anti-inflammatory activities and tissue regeneration capabilities shown by MSCs [20]. Therefore, exosomes isolated from MSCs are currently attracting attention as an alternative to MSC-based therapy, because they pose lower risks in terms of adverse effects while retaining the therapeutic efficacy of MSCs [21]. For example, exosomes have a low risk of tumor formation without self-replication and do not induce immune responses [22]. In addition, because exosomes are much smaller than cells (ranging from 20 to 200 nm), their administration does not induce embolism, which is a potential risk associated with cell therapy [23]. Currently, attempts are being made to treat AD using exosomes derived from MSCs [24]. To this end, various methods are being tried to precondition MSCs and enhance the therapeutic efficacy of MSC-derived exosomes [25]. For example, $CoCl_2$ can induce hypoxic conditioning by increasing HIF-1 [26], and it has indeed been reported that MSCs preconditioned with $CoCl_2$ showed enhanced therapeutic effects, such as the reduction of oxidative stress and inflammation in a TNF-α/IFN-γ-induced inflammation cell model [27, 28]. It is yet to be tested whether exosomes isolated from MSCs preconditioned with $CoCl_2$ exert antiatopic effects in an *in vivo* AD model.

In this study, we isolated $CoCl_2$-treated MSC-derived exosomes (Chem-exo) and *in vitro* and *in vivo* experiments were conducted to evaluate the anti-inflammatory and anti-AD efficacies of Chem-exo.

Materials and Methods

1. Cell culture and treatment

HaCaT (human keratinocyte cell line) cells were maintained in high glucose DMEM medium (WelGENE Inc., Daegu, Korea) containing 10% fetal bovine serum (Corning Inc., Corning, NY, USA), 1% penicillin/streptomycin (WelGENE Inc.) at 37℃ in a humidified 5% CO_2 incubator. For *in vitro* experiments, the HaCaT cells were washed with PBS, exchanged with media containing 5% exosome-depleted FBS, and activated with lipopolysaccharide (LPS, 100 μg/mL) (Sigma-Aldrich) and Interferon-γ (IFN-γ, 100 ng/mL) (PeproTech, Rocky Hill, NJ, USA). Human bone marrow-derived mesenchymal stem cells (MSCs) were maintained in low glucose DMEM medium containing 10% FBS and 1% penicilin/steptomycin at 37°C in a humidified 5% CO_2 incubator. Low glucose DMEM medium without FBS was used for exosome isolation. To enhance the anti-inflammatory function, cobalt chloride ($CoCl_2$) was added in the MSC medium for 24 h. Mesenchymal stem cells were kindly gifted from Samsung Medical Center, and the Institutional Review Board of Samsung Medical Center approved studies and all samples were obtained with informed consent

2. Exosome isolation and characterization

The MSC-cultured medium was collected and centrifuged for 10 min at 2,000 g and 4°C to remove debris and was then passed through a 0.22-μm filter. To isolate exosomes from MSCs, the filtered medium was run with the LabSpinner™ (ExoDiscovery, Ulsan, Korea) based on size exclusion method. After washing twice with PBS, the exosome sample was eluted with 200 μl of PBS, aliquoted, and stored at − 20°C until use. Exosome size and concentration were measured using a NanoSight 300 particle size analyzer (Malvern Instruments, Malvern, UK).

For Western blot analysis, the exosomes were lysed using RIPA buffer and Laemmli loading buffer. Proteins were separated by 10% sodium dodecyl sulphate-polyacrylamide gel electrophoresis, transferred to a polyvinylidene fluoride membrane, blocked with 5% skim milk for 1 h, and incubated with antibodies overnight (Table S1). The membrane was washed and incubated with horseradish peroxidase (HRP)-conjugated secondary antibodies for 1 h. Blots were visualized with ECL (Thermo Fisher Scientific, Cleveland, OH, USA) as per the manufacturer's instructions. Exosomes at a concentration of $1x10^8$/well were tested in the *in vitro* experiments.

3. Characterization of MSCs

MSCs were trypsinized and washed prior to resuspension in PBS and then adjusted to 100 μl of cell suspension. For cell surface labeling, cell suspensions were incubated at 4°C for 30 min with 1 μl of antibodies against MSC-specific surface markers (Table S2). Cell surface marker analysis was performed using an Attune NxT Flow Cytometer (Thermo Fisher Scientific).

4. CCK8 assay for MSC viability

MSCs were cultured in low-glucose DMEM medium supplemented with 10% FBS and 1% penicillin/streptomycin at 37°C and 5% CO_2. A total of 1×10^4 MSCs were seeded in a 96-well plate and cultured overnight at 37°C for cell attachment. Subsequently, $CoCl_2$ was applied at concentrations of 200 μM, 400 μM, 800 μM, and 1,600 μM, and then reacted with 10 μl of CCK8 reagent for 24 h. Cell viability was analyzed by measuring absorbance through a microplate reader at a wavelength of 450 nm.

5. Cell proliferation assay

A total of 1×10^4 MSCs were seeded in a 96-well plate and incubated at 37°C overnight for cell attachment. Then, 10 μl of CCK8 reagent (Dojindo Molecular Technologies Inc., Kumamoto, Japan) was applied for 24 h after 200, 400, 800 and 1600μM of CoCl2 treatment. A total of 1×10^4 HaCaT cells were seeded in a 96-well plate and incubated at 37°C overnight for cell attachment. Then, 10 μl of CCK8 reagent (Dojindo Molecular Technologies Inc.) was applied for 24 h after the LPS, dexamethasone, and exosome (2×10^7 particles) treatments. Absorbance was recorded using a microplate reader at a wavelength at 450 nm.

6. Wound healing assay

HaCaT cells at a concentration of 1×10^5/well were seeded in a 12-well culture plate and cultured for 2 days. Wounds were made by scraping the surface with a 1-mL pipette tip. After washing with PBS,

photographs of the wounds were taken at 0, 24, 48, and 72 h by light microscopy. Wound healing was measured by comparing the widths of lesions at 0 h with those at each subsequent time using ImageJ (NIH, Bethesda, MD, USA)

7. Quantitative real-time PCR (qRT-PCR) for in vitro experiments

HaCaT cells at a concentration of $1 \times 10_5$/well were seeded in a 12-well culture plate and cultured for 3 days. IFN-γ (100 ng/mL), LPS (100 μg/mL), dexamethasone (100 ng/mL), and exosome (1×10^8 particles/well) treatments were carried out for 24 h. For gene expression analysis, RNA was extracted using the MiniBEST Universal RNA Extraction Kit (TaKaRa, Otsu, Shiga, Japan), and cDNA was synthesized using the PrimeScript™ 1st strand cDNA Synthesis Kit (TaKaRa) according to the manufacturer's instructions. TOPreal™ qPCR 2X 2x PreMIX (Enzynomics, Daejeon, Korea) was used for qRT-PCR, which was carried out on a StepOnePlus Real-Time PCR System (Thermo Fisher Scientific). The primers used are listed in Table S3.

8. Animals

25 of Eight-week-old male BALB/C mice purchased from Orientbio (Sungnam, Korea) were habituated for a week in a controlled environment at a temperature of 22˚C ± 2˚C and humidity of 50 ± 10% under a 12 h light/dark cycle. Standard laboratory chow and water were provided ad libitum. The maintenance of mice and experiments conducted on them complied with the Guide for the Care and Use of Laboratory Animals issued by the National Institute of Health (publication No. 85 – 23, revised 1996). Approval was obtained by the Institutional Animal Care and Use Committee of the Korea Institute of Science and Technology (Certification No. KIST-2018-092) before conducting the experiments. Also, the animal study was conducted in accordance with ARRIVE guidelines.

9. Induction of AD-like symptoms in mice using oxazolone and $CoCl_2$-exosome treatment

The experimental mice were randomly divided into five groups(n = 5): (1) NC group; non-treatment, (2) OXA group; 0.1% oxazolone treatment, (3) Dexa group; 0.1% oxazolone and dexamethasone (20 μL, 10 mg/kg) treatment, (4) Ctrl-exo group; 0.1% oxazolone and control-exosome (20 μL, 2×10^9 particles) treatment, and (5) Chemo-exo group; 0.1% oxazolone and $CoCl_2$-exosome (20 μL, 2×10^9 particles) treatment. To induce the first AD-like lesions, 20 μL of 1% oxazolone dissolved in acetone/olive oil (4:1, v/v) was topically applied to the mice's ears. A week later, 0.1% oxazolone (20 μL) was applied to the ears at 2-day intervals for 3 weeks, and during these 3 weeks, control-exosome, $CoCl_2$-exosome, or dexamethasone were also intradermally injected in the ears every 2 days. Throughout the experiment, ear thickness was measured three times each week using calipers.

10. Histopathological examination

Ear skin samples obtained from the BALB/c mice were fixed in 10% formalin for 24 h. The fixed skin samples were embedded in paraffin and sectioned (5 μm), and paraffin was removed 3 min/3 times using

a xylene solution (Junsei, Tokyo, Japan). Then, the sections were hydrated in 100%, 95%, 70%, and 50% ethanol for 1 min and subsequent histopathological experiments were performed in the same manner.

10.1. Hematoxylin and eosin (H&E) staining

H&E staining was performed to measure the dermatological phenotypes. Ethanol, acetic acid, and glycerol were added to a 10% ammonium solution to obtain a hematoxylin (Sigma-Aldrich, St. Louis, Mo, USA) solution. The paraffin-free tissue slides were stained with hematoxylin for 10 min. Then, the stained slides were washed in distilled water for 1 min, immersed in 1% HCl and 70% ethanol for 5 s, and then immersed in distilled water for 5 min. Subsequently, the slides were treated with 0.3% aqueous ammonia for 2 min and washed with distilled water. The washed tissue was stained with 1% eosin (Sigma-Aldrich) for 2 min, followed by dehydration in 50%, 70%, 90%, and 100% ethanol. Each slide was washed three times in a xylene solution for 3 min. A mounting solution (Canada balsam, Sigma-Aldrich) was applied on each washed slide, and cover slides were put in place to allow hardening. Then, the epidermal thickness of the ear tissue was measured using an Olympus microscope (CX43, Olympus Optical Co., Tokyo, Japan) and Cellsens standard (Olympus Optical Co.) software.

10.2. Toluidine blue staining

Toluidine blue staining was performed to evaluate the infiltration of mast cells in the ear dermis. A toluidine blue stock solution was prepared by mixing toluidine blue O and 70% ethanol (1%, w/v). A toluidine blue working solution was then prepared by mixing 5 mL of toluidine blue stock solution and 1% sodium chloride in D.W (w/v) and was adjusted to pH 2.3. Then, the paraffin-free tissue slides were stained using the toluidine blue working solution for 3 min and were subsequently washed in PBS for 5 min. After dehydration in 95% ethanol for 1 s, in 100% Et-OH for 10 dips, and in xylene for 3 min three times, the slides were mounted with Permount mounting medium (Fisher chemical, Hampton, NH, USA) and cover-slipped. All slides were analyzed using a light microscope (CX43, Olympus Optical Co.) and photographed (TE-2000U, Nikon Instruments Inc., Melville, USA).

10.3. Immunofluorescence (IF) test

Antigens were retrieved from each slide using Tris-EDTA buffer (pH 9.0). Then, the paraffin-free tissue slides were sequentially blocked with 5% BSA (phosphate-buffered saline containing 0.05% TWEEN 20, PBST) for 1 h and incubated with keratin 10, involucrin, or filaggrin overnight. Appropriate secondary antibodies were then probed, and the slides were mounted with VECTASHIELD containing DAPI (Vector Laboratories Inc, CA, USA) and examined under a Nikon Eclipse TE2000U microscope (Nikon Corporation, Tokyo, Japan). The information about all the antibodies used for IF testing is included in Table S4.

10.4. 3, 3'-diaminobenzidine (DAB) staining

Antigens were retrieved using microwave with TRIS-EDTA buffer (pH 9.0). Then, the paraffin-free tissue slides were treated with 3% hydrogen peroxide in PBS for 15 min. After this treatment, the slides were first incubated with 2% BSA in PBS as a blocking reagent for 1 h at room temperature and then with CD4, CD45, CD3, or F4/80 antibody overnight at 4°C. After washing with PBS, the slides were subsequently

incubated with appropriate secondary antibodies for 2 h at room temperature and stained with 3, 3'-diaminobenzidine tetrachloride (Vector Laboratories, Burlingame, CA, USA) for 1 min. Finally, the slides were stained again with hematoxylin for 30 s, mounted with Permount mounting medium (Fisher chemical, Hampton, NH, USA), and cover-slipped. All slides were analyzed using a light microscope (CX43, Olympus Optical Co.) and photographed (TE-2000U, Nikon Instruments Inc., Melville, USA). The information about all the antibodies used in DAB staining is included in Table S5.

11. Quantitative real-time PCR (qRT-PCR) for in vivo experiments

Fresh skin tissue was homogenized with Biomasher (Nippi, Tokyo, Japan), and total RNA was extracted using the RNeasy® Mini kit (Qiagen, Hilded, Germany). The extracted total RNA was reverse-transcribed into cDNA using the RevertAid First Strand cDNA Synthesis Kit (Thermo Fisher Scientific). The synthesized cDNA (1 μg) was added to the Power-Up SYBR Green Master mix (Thermo Fisher Scientific) at an appropriate ratio and the PCR was run on an AP7500 qRT-PCR System (Thermo Fisher Scientific). The PCR steps consisted of an initial holding stage at 50˚C for 2 min and at 95˚C for 20 s followed by a cycling stage with 40 cycles at 95˚C for 20 s and at 57˚C for 1 min. Glyceraldehyde 3-phosphate dehydrogenase (GAPDH) gene was used as a housekeeping gene and internal standard to normalize the expression of primers. Based on the qRT-PCR results, the relative expression of target genes for different groups was calculated using the $2^{-\Delta\Delta CT}$ method [29]. The primers used are listed in Table S6.

12. Statistical analysis

Statistical analysis of the data was conducted in IBM SPSS version 24.0 (SPSS Inc., Chicago, IL, USA). Differences between multiple groups were analyzed using one-tailed analysis of variance (ANOVA) followed by Tukey's post-hoc test ($p < 0.05$). All experiments were independently conducted at least three times. The values for each experiment are presented as the mean ± standard deviation (SD) of the three measurements.

Results

1. Effects of $CoCl_2$ treatment on the functions of MSC-derived exosomes

$CoCl_2$ is known to induce HIF1α, mimicking hypoxic conditioning [30]. MSCs preconditioned with $CoCl_2$ have shown reduced oxidative stress and inflammation in a TNF-α/IFN-γ-induced inflammation cell model [27]. As the $CoCl_2$ treatment has been shown to have beneficial effects on the therapeutic activities of MSCs [28], these were treated with $CoCl_2$ to test whether the anti-inflammatory activity of exosomes derived from MSCs could be enhanced. Before testing this hypothesis, we first investigated whether the $CoCl_2$ treatment affected cell viability and the characteristics of MSCs. $CoCl_2$ was shown to increase the proliferation of MSCs in a dose-dependent manner, reaching the maximum increase at a concentration of 800 μM (Fig. 1A), while flow cytometry analysis showed that the $CoCl_2$ treatment did not change the

expression of surface proteins (Fig. 1B). These data indicated that preconditioning MSCs with $CoCl_2$ did not affect cell viability or marker expression. Therefore, we proceeded to test the therapeutic effects of exosomes. To this end, exosomes were isolated from MSCs, their size and marker expression were assessed, and their therapeutic activities were tested. Exosomes derived from naïve MSCs (Ctrl-exo) and $CoCl_2$-treated MSCs (Chem-Exo) showed a similar size distribution (Fig. 1C). Western blot analysis confirmed the expression of exosomal markers CD63, CD81, TSG101, and CD9, and the lack of expression of negative markers on the Ctrl-exo and Chem-exo groups (Fig. 1D).

One of the effects of AD is the disruption of the skin barrier. To repair the damage, it is essential to quickly restore the damaged epidermal layer by ensuring the migration and proliferation of keratinocytes. Migrated keratinocytes prevent further inflammation [31]. We tested the proliferation and migration of HaCaT, a human keratinocyte cell line, under exosome treatment (Fig. 2A, B). LPS was added to HaCaT cells to mimic the inflammation-induced cell damage in AD. The proliferation of HaCaT cells decreased under the LPS treated condition (Fig. 2A). Increased cell proliferation and migration were observed in both the Ctrl-exo and Chem-exo groups (Fig. 2A, B). To assess whether the Chem-exo treatment could reduce the AD phenotypes, we tested its anti-inflammatory effects *in vitro* (Fig. 2C). Inflammation was induced using LPS or IFN-γ in HaCaT cells, which caused the upregulation of inflammatory cytokines and chemokines (Fig. 2C). The dexamethasone treatment was shown to decrease the inflammatory factors (Fig. 2C), while the Ctrl-exo and Chem-exo treatments reduced the expression of inflammatory cytokines and chemokines (Fig. 2C). Chem-exo was more successful than Ctrl-exo in reducing IL-6, IL-33, monocyte chemoattractant protein-1 (MCP-1), CC motif chemokine ligand 17 (CCL17), and CCL22 (Fig. 2C). The level of IL-10, an anti-inflammatory cytokine, increased in the Chem-exo-treated HaCaT cells (Fig. 2C).

The above results indicated that exosomes derived from MSCs promoted keratinocyte proliferation and migration. In addition, the Chem-exo treatment was shown to be more effective than the Ctrl-exo treatment.

2. Therapeutic effects of exosomes derived from $CoCl_2$-treated MSCs in the OXA-induced AD mouse model

The Chem-exo treatment increased the proliferation and migration of HaCaT cells *in vitro* (Fig. 2A, B) and also reduced the expression of inflammatory cytokines and chemokines (Fig. 2C). Based on the *in vitro* data, we hypothesized that Chem-exo might ameliorate AD phenotypes also *in vivo*. To test this hypothesis, AD was induced by administering OXA to BALB/c mice for 4 weeks (Fig. 3A). The OXA-treated group developed AD-like skin symptoms such as ear swelling and erythema. However, those symptoms were reduced in the Dexa- or Chem-exo-treated groups (Fig. 3B).

During the experimental period, ear thickness continuously increased in the OXA-treated group compared with the non-treated group (Fig. 3C). On day 28, ear thickness in the Ctrl-exo-treated group was similar to that in the OXA-treated group, while the Dexa- and Chem-exo-treated groups showed a significantly decreased ear thickness (Fig. 3D). H&E staining was performed to evaluate the effects of Chem-exo on

the histology of the mice's ears. The results showed that the ear epidermis was thicker in the OXA-treated group than in the non-treated group (Fig. 3E). The Ctrl-exo treatment did not decrease the ear's epidermal thickness whereas the Dexa and Chem-exo treatments did (Fig. 3E). By measuring the ear's epithelial thickness it was confirmed that Chem-exo decreased ear thickness (Fig. 3G). Toluidine blue staining showed that the infiltration of mast cells increased in the OXA-treated group (Fig. 3F, H), while the mast cell number remained stable in the groups treated with Ctrl-exo and Chemo-exo (Fig. 3F, H).

To investigate the effect of Chem-exo on the restoration of the abnormal expression of skin barrier proteins in the ear epidermis caused by OXA, we analyzed epidermal differentiation markers, i.e., filaggrin (FLG), involucrin (INV), and keratin 10 (K10). The normal expression of all the skin barrier markers was properly controlled and positioned without disruption (Fig. 4A) [32]. The Chem-exo- and Dexa-treated groups showed a similar reduction in the abnormal expression of FLG (Fig. 4A). Moreover, Chem-exo restored decrease in INV expression induced by OXA (Fig. 4A). In addition, the expression pattern of K10 in the OXA-treated group was different from that in the non-treated group. The pattern was restored in the Chem-exo-treated group (Fig. 4A). These data suggested that Chem-exo can be used to treat damaged epidermis structures as it induces the restoration of disrupted skin barrier proteins.

To determine the anti-inflammatory effect of Chem-exo in the OXA-treated AD mouse model, the expression of cytokines and chemokines was measured via qRT-PCR. The mRNA expression of IL-1β, IL-4, IL-6, IL-17A, CCL17, S100 calcium binding protein A7 (S100A7), S100A8, and S100A9 in the OXA-treated group significantly increased compared with that in the non-treated group (Fig. 4B). The Ctrl-exo-treated group showed a decrease in the expression of IL-6 and S100A7. Overall, Chem-exo reduced the expression of all mRNAs except for IL-4, and CCL17 (Fig. 4B).

3. Effects of exosomes derived from $CoCl_2$-treated MSCs on immune cell infiltration in the OXA-induced AD mouse model

In AD, immune cells such as helper T cells, leukocytes, and macrophages are infiltrated into the dermis, and inflammatory responses are triggered by keratinocytes due to cytokines and chemokines released from immune cells [33]. As a result of the recruitment of immune cells in the dermis, the symptoms of AD are amplified, leading to an increase of pro-inflammatory signals [34]. In this study, we examined whether Chem-exo can affect leukocyte infiltration in the OXA-induced AD mouse model. The CD4, CD45, CD3, and F4/80 positive cells were shown to significantly infiltrate into the dermis in the OXA-treated group compared with the non-treated group (Fig. 5A, B). The CD4 positive cells were upregulated in the OXA-treated group compared with those in the non-treated group. The level of infiltration of CD4 positive cells in the Ctrl-exo group remained stable while it increased in the OXA-treated group. However, Chem-exo reduced the infiltration of CD4 positive cells (Fig. 5A, B). The infiltration of CD45 cells increased in the OXA- and Ctrl-exo-treated groups, but it decreased in the dermis of the Chem-exo-treated group (Fig. 5A, B). In addition, only the Chem-exo treatment showed a decrease in the infiltration of CD3 and F4/80 cells (Fig. 5A, B).

Discussion

Exosomes released from producer cells, which act as paracrine mediators between parent and target cells, deliver mRNA, microRNA, and proteins to target cells [35]. In particular, similarly to MSCs, MSCs-derived exosomes have been reported to have various therapeutic effects, including anti-diabetes, anti-chronic kidney disease, anti-inflammatory, anti-aging, and wound healing effects [36, 37]. Attempts have been made to improve the therapeutic activities of exosomes by inducing cytokines, chemicals, growth factors, and hypoxic conditions [38, 39]. Hypoxic conditioning has been shown to enhance the therapeutic effects of MSCs by stimulating proliferation and migration and at the same time suppressing the inflammation and apoptosis of target cells [40]. In addition, biogenesis and the release of exosomes are promoted in hypoxia-conditioned MSCs [41, 42]. Exosomes are currently being tested to treat AD. In particular, exosomes derived from MSCs found in human adipose tissue were shown to alleviate AD phenotypes [43]. A disrupted epidermal barrier in AD is restored by the *de novo* synthesis of ceramides induced by the MSC-derived exosomes [44]. It has also been shown that exosomes in which miR 147a was overexpressed suppressed inflammatory injury in an AD mouse model [45].

In this study, we used $CoCl_2$ to induce hypoxic conditioning. The data showed that treating MSCs with $CoCl_2$ had no effects on their properties and derived exosomes. Chem-exo were similar to those of Ctrl-exo in terms of particle size and marker expression. Moreover, the $CoCl_2$ treatment increased the proliferation of MSCs in a concentration-dependent manner.

The most prominent manifestations of AD are inflammation and disruption of the skin barrier. The Chem-exo treatment showed an enhanced proliferation and migration of human keratinocyte HaCaT cells *in vitro*. Under inflammatory conditions, Chem-exo reduced the expression of inflammatory cytokines and chemokines in HaCaT cells *in vitro*. In the OXA-induced AD mouse model, the Chem-exo treatment reduced ear thickness and epidermal thickness as well as the infiltration of mast cells into the dermis. Interestingly, the Chem-exo treatment restored the epidermal discrimination markers which had been disrupted in the OXA-treated group. The treatment also reduced the infiltration of CD4 and CD45 positive cells as well as the expression of inflammatory cytokines and chemokines *in vivo*. These data indicated that the hypoxic conditioning of MSCs induced by $CoCl_2$ enhanced the efficacy of exosomes in treating AD. Further studies are necessary to confirm the key factors of Chem-exo that exert anti-atopic effects. To adopt MSC-derived exosomes as a therapy, it is necessary to develop strategies for enhancing their therapeutic efficacy. In this regard, in addition to hypoxic preconditioning, surface modifications are currently being tested to enhance the therapeutic activity of exosomes [46]. For example, glycosylation has been shown to alter the biodistribution of injected exosomes [47, 48]. By combining preconditioning and surface engineering techniques, it may be possible to produce clinically available exosomes [49]. In conclusion, our study recommends the application of exosomes to treat AD.

Declarations

Conflict of Interest

The authors declared no potential conflicts of interest.

Author Contribution

Jin-Woo Kim: conception, literature review, figure design, manuscript writing, and editing; Hyunji Lee: literature review, figure design, manuscript writing; Jung Min Lee: conception, literature review, figure design, manuscript writing, editing, and final approval; Jin-Chul Kim: conception, literature review, figure design, manuscript writing, editing, and final approval.

Acknowledgments

Jin-Woo Kim and Hyunji Lee contributed equally to this work. Graphical abstract was created with BioRender.com

Data Availability

The data of this study are available from the corresponding author upon reasonable request.

References

1. Nutten, S. Atopic dermatitis: global epidemiology and risk factors. *Ann. Nutr. Metab.* 66 Suppl 1, 8-16. https://doi.org/10.1159/000370220 (2015).
2. Eichenfield, L.F. *et al*. Guidelines of care for the management of atopic dermatitis: Section 1. Diagnosis and assessment of atopic dermatitis. *J. Am. Acad. Dermatol.* 70(2), 338-351. https://doi.org/10.1016/j.jaad.2013.10.010 (2014).
3. Asher, M.I. *et al*. Worldwide time trends in the prevalence of symptoms of asthma, allergic rhinoconjunctivitis, and eczema in childhood: ISAAC Phases One and Three repeat multicountry cross-sectional surveys. *Lancet* 368(9537), 733-743. https://doi.org/10.1016/S0140-6736(06)69283-0 (2006).
4. Honda, T., Egawa, G., Grabbe, S., & Kabashima, K. Update of immune events in the murine contact hypersensitivity model: toward the understanding of allergic contact dermatitis. *J. Invest. Dermatol.* 133(2), 303-315. https://doi.org/10.1038/jid.2012.284 (2013).
5. Leung, D.Y. Pathogenesis of atopic dermatitis. *J. Allergy. Clin. Immunol.* 104(3), S99-S108. https://doi.org/10.1016/S0091-6749(99)70051-5 (1999).
6. Salimi, M. *et al*. A role for IL-25 and IL-33-driven type-2 innate lymphoid cells in atopic dermatitis. *J. Exp. Med*. 210(13), 2939-2950. https://doi.org/10.1084/jem.20130351 (2013).

7. Moreno, A. S., McPhee, R., Arruda, L. K., & Howell, M. D. Targeting the T helper 2 inflammatory axis in atopic dermatitis. *Int. Arch. Allergy Immunol.* 171(2), 71-80. https://doi.org/10.1159/000451083 (2016).
8. Maggi, L. *et al*. Human circulating group 2 innate lymphoid cells can express CD154 and promote IgE production. *J. Allergy Clin. Immunol.* 139(3), 964-976. https://doi.org/10.1016/j.jaci.2016.06.032 (2017).
9. Watanabe, R. *et al*. Human skin is protected by four functionally and phenotypically discrete populations of resident and recirculating memory T cells. *Sci. Transl. Med.* 7(279), 279ra239. https://doi.org/10.1126/scitranslmed.3010302 (2015).
10. Atherton, D. J. Topical corticosteroids in atopic dermatitis. *BMJ* 327(7421), 942-943. https://doi.org/10.1136/bmj.327.7421.942 (2003).
11. Yasir, M. *et al*. Corticosteroid adverse effects. 2018.
12. Weiss, A.R.R., & Dahlke, M. H. Immunomodulation by mesenchymal stem cells (MSCs): Mechanisms of action of living, apoptotic, and dead MSCs. *Front. Immunol.* 10, 1191. https://doi.org/10.3389/fimmu.2019.01191 (2019).
13. Fu, Y. *et al*. Trophic effects of mesenchymal stem cells in tissue regeneration. *Tissue Eng. Part B Rev.* 23(6), 515-528. https://doi.org/10.1089/ten.TEB.2016.0365 (2017).
14. DiMarino, A. M., Caplan, A. I., & Bonfield, T. L. Mesenchymal stem cells in tissue repair. *Front. Immunol.* 4, 201. https://doi.org/10.3389/fimmu.2013.00201 (2013).
15. Sargent, A., & Miller, R. H. MSC therapeutics in chronic inflammation. *Curr. Stem Cell Rep.* 2(2), 168-173. https://doi.org/10.1007/s40778-016-0044-6 (2016).
16. Shin, T. H., Kim, H. S., Choi, S. W., & Kang, K. S. Mesenchymal stem cell therapy for inflammatory skin diseases: Clinical potential and mode of action. *Int. J. Mol. Sci.* 18(2), 244. https://doi.org/10.3390/ijms18020244 (2017).
17. Musial-Wysocka, A., Kot, & M., Majka, M. The pros and cons of mesenchymal stem cell-based therapies. *Cell Transplant.* 28(7), 801-812. https://doi.org/10.1177/0963689719837897 (2019).
18. Gurunathan, S., Kang, M. H., Jeyaraj, M., Qasim, M., & Kim, J. H. Review of the isolation, characterization, biological function, and multifarious therapeutic approaches of exosomes. *Cells* 8(4), 307. https://doi.org/10.3390/cells8040307 (2019).
19. Kim, D. K., Lee, J., Simpson, R. J., Lötvall, J., & Gho, Y. S. EVpedia: A community web resource for prokaryotic and eukaryotic extracellular vesicles research. *Semin. Cell Dev. Biol.* 40, 4-7. https://doi.org/10.1016/j.semcdb.2015.02.005 (2015).
20. Mashouri, L. *et al*. Exosomes: Composition, biogenesis, and mechanisms in cancer metastasis and drug resistance. *Mol. Cancer* 18(1), 75. https://doi.org/10.1186/s12943-019-0991-5 (2019).
21. Sarvar, D. P., Shamsasenjan, K., & Akbarzadehlaleh, P. Mesenchymal stem cell-derived exosomes: New opportunity in cell-free therapy. *Adv. Pharm. Bull.* 6(3), 293. https://doi.org/10.15171/apb.2016.041 (2016).

22. Shiue, S. J. *et al*. Mesenchymal stem cell exosomes as a cell-free therapy for nerve injury–induced pain in rats. *Pain* 160(1), 210-223. https://doi.org/10.1097/j.pain.0000000000001395 (2019).
23. Vizoso, F. J., Eiro, N., Cid, S., Schneider, J., & Perez-Fernandez, R. Mesenchymal stem cell secretome: Toward cell-free therapeutic strategies in regenerative medicine. *Int. J. Mol. Sci.* 18(9), 1852. https://doi.org/10.3390/ijms18091852 (2017).
24. Ha, D. H. *et al*. Mesenchymal stem/stromal cell-derived exosomes for immunomodulatory therapeutics and skin regeneration. *Cells* 9(5), 1157. https://doi.org/10.3390/cells9051157 (2020).
25. Chen, S., Sun, F., Qian, H., Xu, W., & Jiang, J. Preconditioning and engineering strategies for improving the efficacy of mesenchymal stem cell-derived exosomes in cell-free therapy. *Stem Cells Int.* 2022, 1779346. https://doi.org/10.1155/2022/1779346 (2022).
26. Zhang, B. *et al*. Cobalt chloride inhibits tumor formation in osteosarcoma cells through upregulation of HIF-1α. *Oncol. Lett.* 5(3), 911-916. https://doi.org/10.3892/ol.2013.1127 (2013).
27. Oh, S. W. *et al*. Cobalt chloride attenuates oxidative stress and inflammation through NF-κB inhibition in human renal proximal tubular epithelial cells. *J. Korean Med. Sci.* 29(Suppl 2), S139-S145. https://doi.org/10.3346/jkms.2014.29.S2.S139 (2014).
28. Kwak, J. *et al*. Cobalt chloride enhances the anti-inflammatory potency of human umbilical cord blood-derived mesenchymal stem cells through the ERK-HIF-1α-MicroRNA-146a-mediated signaling pathway. *Stem Cells Int.* 2018, 4978763 https://doi.org/10.1155/2018/4978763 (2018).
29. Livak, K. J., & Schmittgen, T. D. Analysis of relative gene expression data using real-time quantitative PCR and the $2^{-\Delta\Delta CT}$ method. *methods* 25(4), 402-408. https://doi.org/10.1006/meth.2001.1262 (2001)
30. Muñoz-Sánchez, J., & Chánez-Cárdenas, M. E. The use of cobalt chloride as a chemical hypoxia model. *J. Appl. Toxicol.* 39(4), 556-570. https://doi.org/10.1002/jat.3749 (2019).
31. Landen, N. X., Li, D., & Stahle, M. Transition from inflammation to proliferation: a critical step during wound healing. *Cell Mol. Life Sci.* 73(20), 3861-3885. https://doi.org/10.1007/s00018-016-2268-0 (2016).
32. Furue, M. Regulation of filaggrin, loricrin, and involucrin by IL-4, IL-13, IL-17A, IL-22, AHR, and NRF2: Pathogenic implications in atopic dermatitis. *Int. J. Mol. Sci.* 21(15), 5382. https://doi.org/10.3390/ijms21155382 (2020).
33. Piipponen, M., Li, D., & Landen, N. X. The Immune functions of keratinocytes in skin wound healing. *Int. J. Mol. Sci.* 21(22), 8790. https://doi.org/10.3390/ijms21228790 (2020).
34. Hennino, A. *et al*. Skin-infiltrating CD8+ T cells initiate atopic dermatitis lesions. *J. Immunol.* 178(9), 5571-5577. https://doi.org/10.4049/jimmunol.178.9.5571 (2007).
35. Asgarpour, K. *et al*. Exosomal microRNAs derived from mesenchymal stem cells: Cell-to-cell messages. *Cell Commun. Signal.* 18(1), 1-16. https://doi.org/10.1186/s12964-020-00650-6 (2020).
36. Mendt, M., Rezvani, K., & Shpall, E. Mesenchymal stem cell-derived exosomes for clinical use. *Bone Marrow Transplant.* 54(Suppl 2), 789-792. https://doi.org/10.1038/s41409-019-0616-z (2019).

37. Ha, D. H. *et al*. Mesenchymal stem/stromal cell-derived exosomes for immunomodulatory therapeutics and skin regeneration. *Cells* 9(5), 1157. https://doi.org/10.3390/cells9051157 (2020).
38. Noronha, N. C. *et al*. Priming approaches to improve the efficacy of mesenchymal stromal cell-based therapies. *Stem Cell Res. Ther.* 10(1), 131. https://doi.org/10.1186/s13287-019-1224-y (2019).
39. Lee, H. *et al*. Cobalt chloride, a hypoxia-mimicking agent, targets sterol synthesis in the pathogenic fungus *Cryptococcus neoformans*. *Mol. microbiol.* 65(4), 1018-1033. https://doi.org/10.1111/j.1365-2958.2007.05844.x (2007).
40. Yang, Y., Lee, E. H., & Yang, Z. Hypoxia-conditioned mesenchymal stem cells in tissue regeneration application. *Tissue Eng Part B Rev.* 28(5), 966-977. https://doi.org/10.1089/ten.TEB.2021.0145 (2022).
41. Zhang, H. C. *et al*. Microvesicles derived from human umbilical cord mesenchymal stem cells stimulated by hypoxia promote angiogenesis both *in vitro* and *in vivo*. *Stem Cells Dev.* 21(18), 3289-3297. https://doi.org/10.1089/scd.2012.0095 (2012).
42. Lin, S., Zhu, B., Huang, G., Zeng, Q., & Wang, C. Microvesicles derived from human bone marrow mesenchymal stem cells promote U_2OS cell growth under hypoxia: the role of PI3K/AKT and HIF-1α. *Hum. cell* 32, 64-74. https://doi.org/10.1007/s13577-018-0224-z (2019).
43. Cho, B. S., Kim, J. O., Ha, D. H., & Yi, Y. W. Exosomes derived from human adipose tissue-derived mesenchymal stem cells alleviate atopic dermatitis. *Stem Cell Res. Ther.* 9(1), 1-5. https://doi.org/10.1186/s13287-018-0939-5 (2018).
44. Shin, K. O. *et al*. Exosomes from human adipose tissue-derived mesenchymal stem cells promote epidermal barrier repair by inducing *de novo* synthesis of ceramides in atopic dermatitis. *Cells* 9(3), 680. https://doi.org/10.3390/cells9030680 (2020).
45. Shi, C. *et al*. Exosomes with overexpressed miR 147a suppress angiogenesis and infammatory injury in an experimental model of atopic dermatitis. *Sci Rep.* 13(1), 8904. https://doi.org/10.1038/s41598-023-34418-y (2023).
46. Pulido-Escribano, V. *et al*. Role of hypoxia preconditioning in therapeutic potential of mesenchymal stem-cell-derived extracellular vesicles. *World J. Stem Cells* 14(7), 453. https://doi.org/10.4252/wjsc.v14.i7.453 (2022).
47. Choi, H. *et al*. Biodistribution of exosomes and engineering strategies for targeted delivery of therapeutic exosomes. *Tissue Eng. Regen. Med.* 18(4), 499-511. https://doi.org/10.1007/s13770-021-00361-0 (2021).
48. Royo, F., Cossío, U., de Angulo, A. R., Llop, J., & Falcon-Perez, J. M. Modification of the glycosylation of extracellular vesicles alters their biodistribution in mice. *Nanoscale* 11(4), 1531-1537. https://doi.org/10.1039/c8nr03900c (2019).
49. Kwak, J. *et al*. Cobalt chloride enhances the anti-inflammatory potency of human umbilical cord blood-derived mesenchymal stem cells through the ERK-HIF-1alpha-MicroRNA-146a-mediated signaling pathway. *Stem Cells Int.* 2018, 4978763. https://doi.org/10.1155/2018/4978763 (2018).

Figures

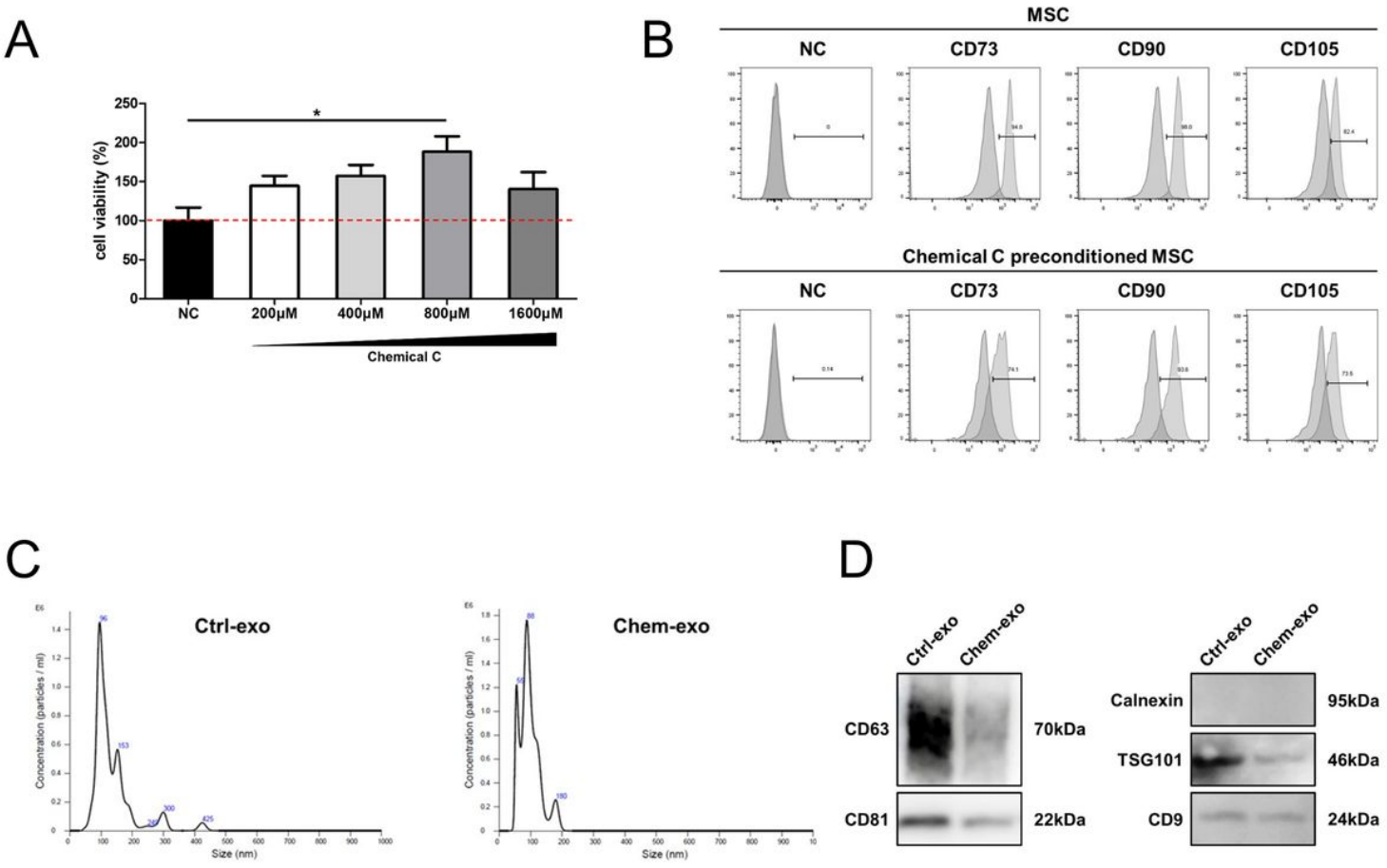

Figure 1

Cell viability and surface marker expression analysis. (A) Viability analysis 24 h after the $CoCl_2$ treatment. Y axis: cell viability (%); X axis: NC: no $CoCl_2$; 200, 400, 800, 1600 μM: concentration of $CoCl_2$ (B) Flow cytometry analysis for MSC markers. Upper: naïve MSCs; lower: $CoCl_2$ treated-MSCs, NC: negative markers-CD34, CD11b, CD19, CD45, HLA_DR. Data represent mean ± SD, n = 3; $^{**}p < 0.01$, $^{*}p < 0.05$ vs. NC. Characterization of Ctrl-exo and Chem-exo. (C) Nanoparticle tracking analysis of Ctrl-exo and Chem-exo. Y axis: particle number; X axis: particle size. (D) Western blot analysis of marker proteins. CD63, CD81, Calnexin, TSG101, and CD9.

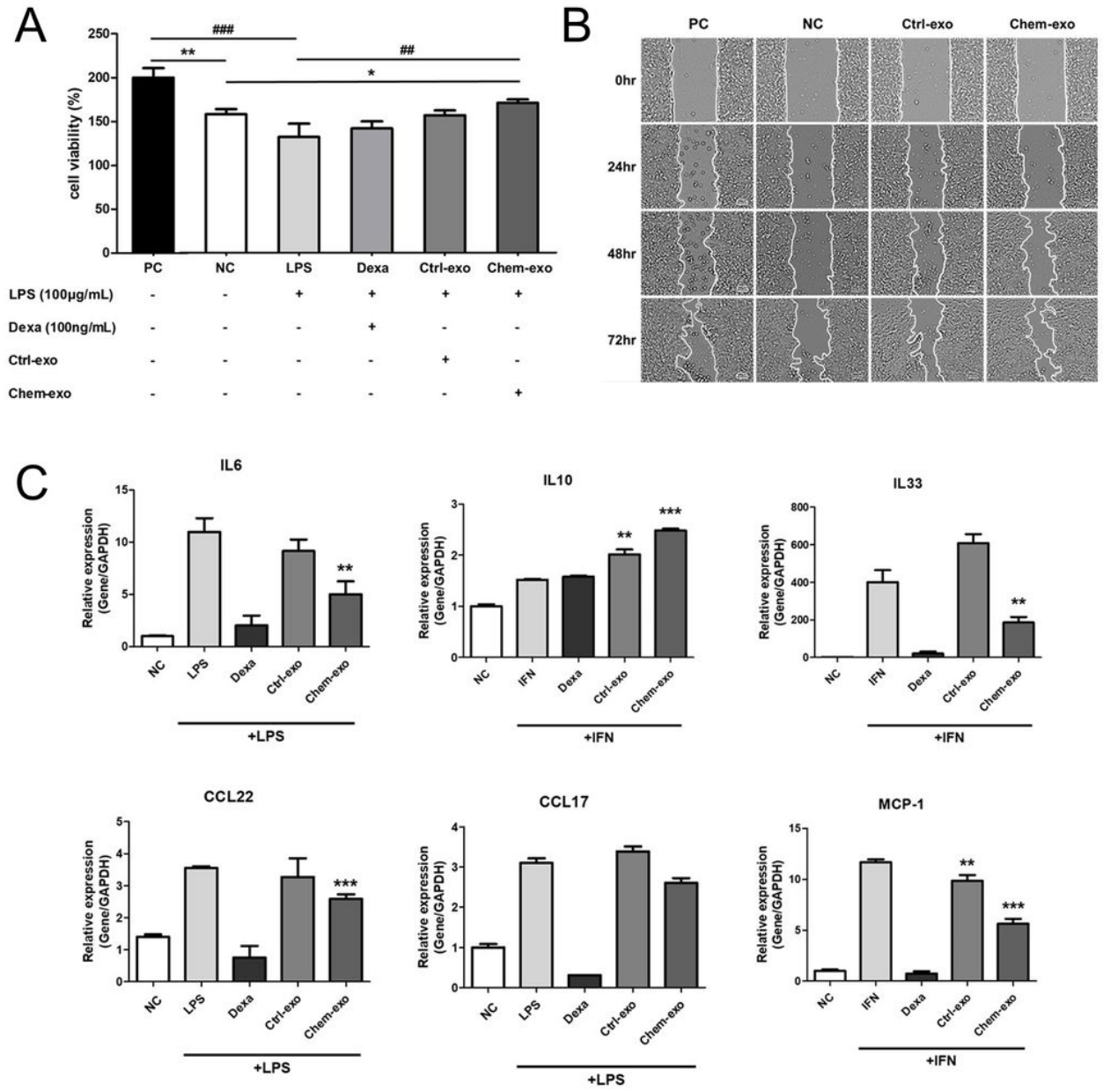

Figure 2

Chem-exo increases the proliferation and migration of HaCaT cells. (A) HaCaT cell proliferation measured via the CCK8 assay. Y axis: cell proliferation (%); X axis: PC: 10% FBS; NC: 5% exosome-depleted FBS; LPS, Dexa, Ctrl-exo, Chem-exo in 5% exosome-depleted FBS. Data represent mean ± SD, n = 3; $^{**}p < 0.01$, $^{*}p < 0.05$ vs. NC, $^{###}p < 0.001$, $^{##}p < 0.01$ vs. LPS. (B) Light microscopy images of the wound healing assay. Pictures were taken at 0, 24, 48, 72 h after wounding. PC: with 10% FBS; NC: with 5% exosome-depleted FBS; Ctrl-exo, Chem-exo in 5% exosome-depleted FBS. Scale bars: 200 μm. (C) qRT-PCR analysis for cytokines and chemokines of HaCaT cells. Concentrations of 100 μg/ml LPS or 100 ng/ml IFN-γ were used to induce inflammation. A total of $1x10^8$ exosome particles was applied during treatments. The expression of each gene was normalized against the expression detected in NC. Data represent mean ± SD, n = 3; $^{***}p < 0.001$, $^{**}p < 0.01$ vs. NC.

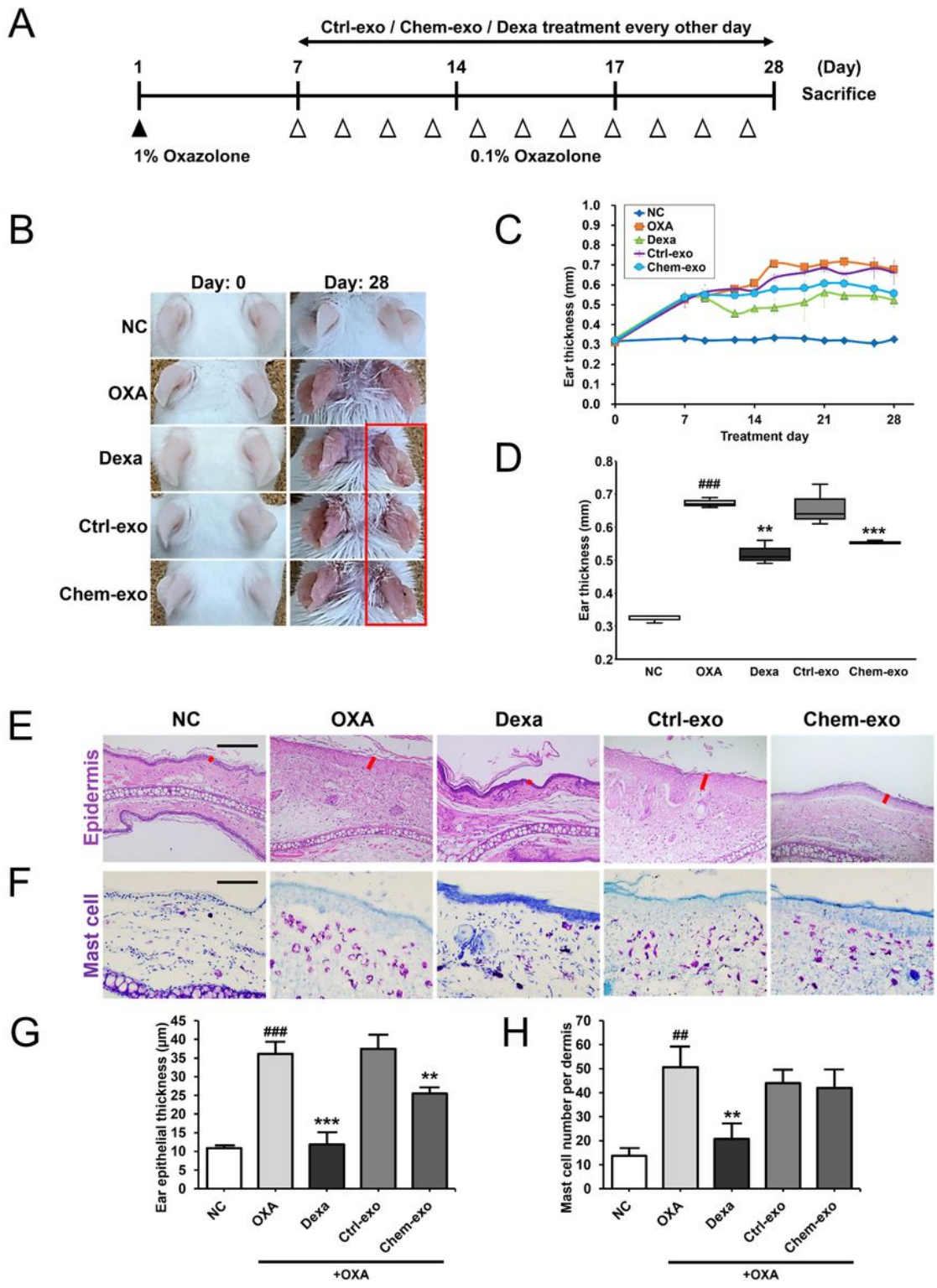

Figure 3

Therapeutic effects of Chem-exo *in vivo*. (A) Schematic figure of experimental schedule. (B) Representative images for measurement of ear thickness. NC: non-treated control group; OXA: oxazolone-treated group; Dexa: dexamethasone-treated group; Ctrl-exo: Ctrl-exo treated group; Chem-exo: Chem-exo treated group. Graph showing ear thickness at (C) days and (D) day 28. (E) Hematoxylin and eosin staining of mouse ear tissue. Red bar: epidermis. Scale bar: 100μm. (F) Toluidine blue staining of mouse

ear tissue. Scale bar: 40μm. Quantitation of (G) ear epidermal thickness and (H) mast cell number per dermis. $^{###}p < 0.001$, $^{##}p < 0.01$ vs NC, $^{***}p < 0.001$, $^{**}p < 0.01$ vs OXA. Data are expressed as the mean ± standard deviation. Statistical significance was analyzed by a one-tailed one-way ANOVA, followed by Tukey's post-hoc test.

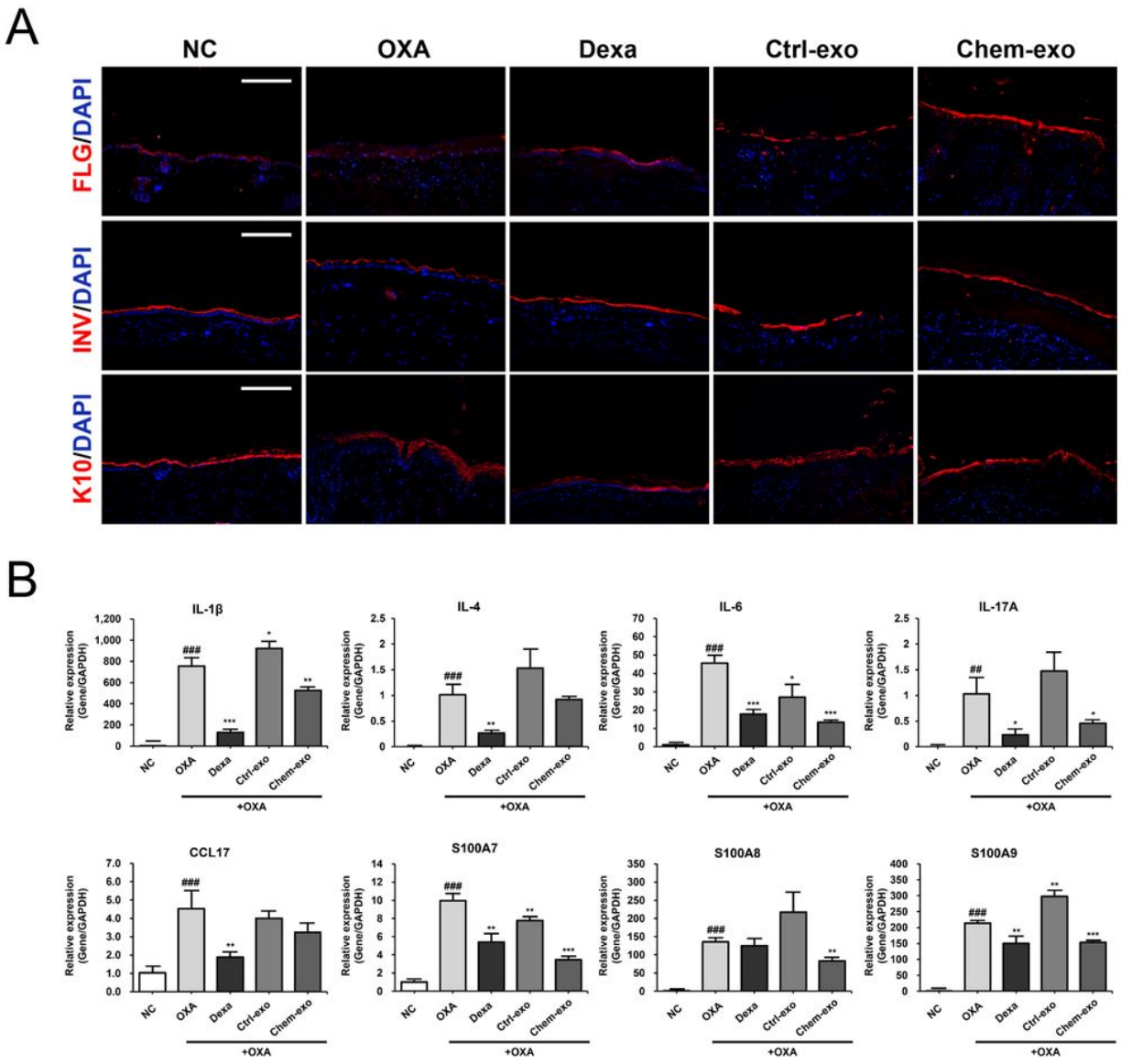

Figure 4

(A) Represented image of the epidermal differentiation makers. Abbreviations: FLG, filaggrin; INV, involucrin; K10, keratin 10. Scale bar, 100 μm. (B) Chem-exo in the regulation of inflammatory cytokines, and chemokines. qRT-PCR analysis of pro-inflammatory cytokines- IL-1β, IL-4, IL-6, IL-17A, and chemokines- CCL17, S100A7, S100A8, S100A9. Abbreviations: NC, non-treated control; OXA, oxazolone-treated; Dexa, dexamethasone-treated; Ctrl-exo, Ctrl-exo-treated; Chem-exo, Chem-exo-treated. $^{###}p < 0.001$, $^{##}p < 0.01$ vs NC, $^{***}p < 0.001$, $^{**}p < 0.01$, $^{*}p < 0.05$ vs OXA. Data are expressed as the mean ± standard

deviation. Statistical significance was analyzed by a one-tailed one-way ANOVA, followed by Tukey's post-hoc test.

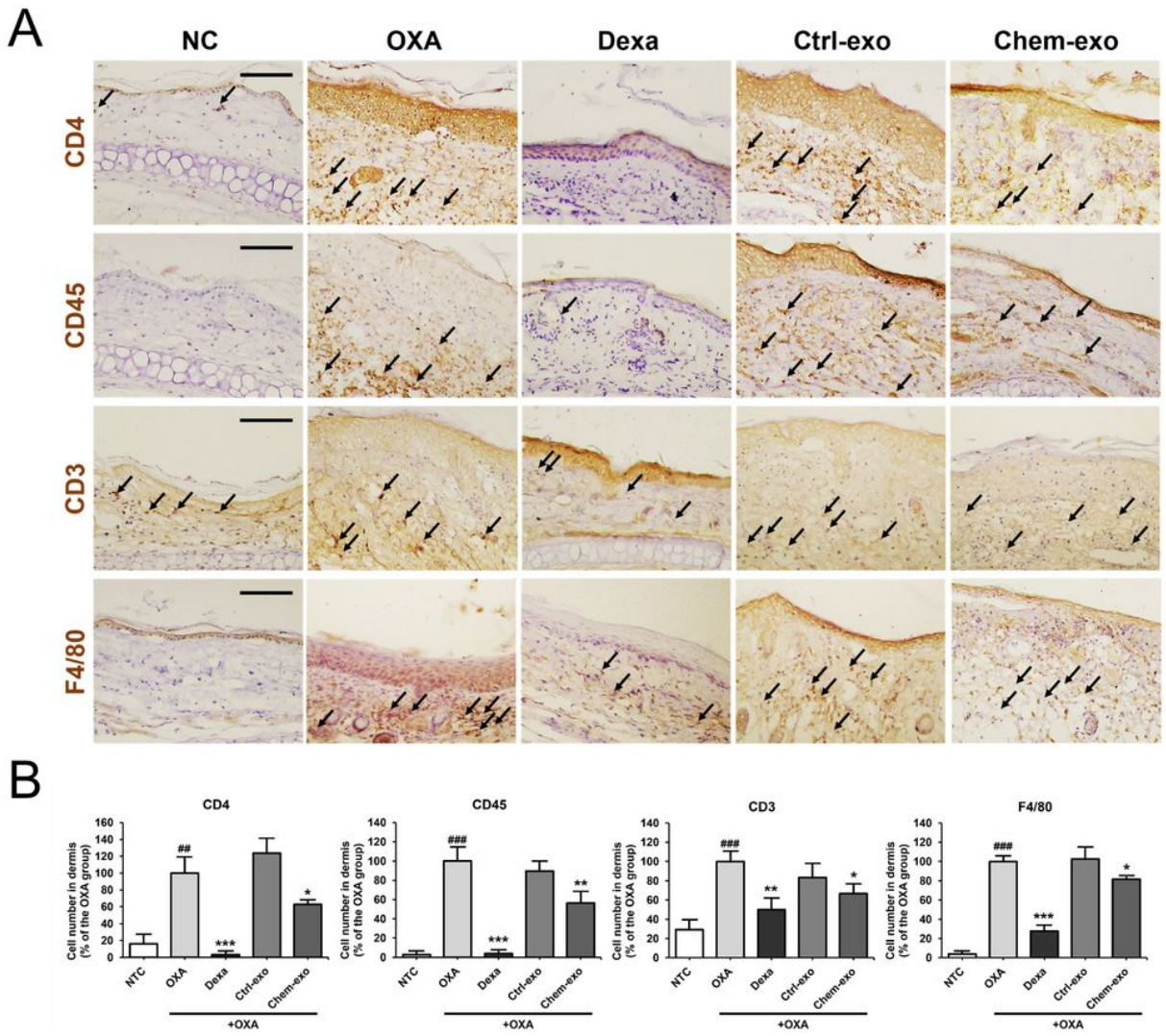

Figure 5

Image depicting immune cells infiltrated into the dermis. CD4, CD45, CD3, and macrophages were observed in the mice's ear tissues. Abbreviations: NC, non-treated control; OXA, oxazolone-treated; Dexa, dexamethasone-treated; Ctrl-exo, Ctrl-exo-treated; Chem-exo, Chem-exo-treated. CD4, helper T cell; CD45, blood cell; CD3, T cell; F4/80, macrophage. Red arrows: target cells in the dermis. Scale bar, 40 μm. Black arrow: immune cells in the dermis. (B) Quantification of CD4, CD45, CD3, and F4/80 cells in the dermis. CD4: helper T cell; CD45: blood cell; CD3: T cell; F4/80: macrophage. Data are expressed as the mean ±SD. Statistical significance was analyzed using the one-tailed one-way ANOVA followed by Tukey's post-hoc test. (C) Effect of Chem-exo on the regulation of inflammatory cytokines and chemokines. qRT-PCR analysis of pro-inflammatory cytokines (IL-6, IL-17, IL-4, and IL-1B) and chemokines (CCL17, S100A7, S100A8, and S100A9). Abbreviations: NC, non-treated control; OXA, oxazolone-treated; Dexa, dexamethasone-treated; Ctrl-exo, Ctrl-exo-treated; Chem-exo, Chem-exo-treated.

Supplementary Files

This is a list of supplementary files associated with this preprint. Click to download.

- SupplementaryMaterials.docx